FAST TRANSONIC CORRECTIONS FOR PANEL METHODS USING VISCOUS-INVISCID INTERACTION

Adrien Crovato[1], Paul Dechamps[1], Alex P. Prado[2], Pedro H. Cabral[2], Vincent E. Terrapon[1] & Grigorios Dimitriadis[1]

[1]University of Liège, Liège, Belgium
[2]Embraer S.A., São José Dos Campos, Brazil

Abstract

This work presents a methodology for quickly computing unsteady aerodynamic loads and flutter in the transonic regime within the context of preliminary aircraft design. The approach relies on correcting an unsteady three-dimensional source and doublet panel method using a recently developed transonic correction technique. The reference steady three-dimensional solutions needed to apply the correction are computed by means of a novel viscous-inviscid interaction scheme, whereby a steady full potential solver is coupled to the unsteady integral boundary layer equations through a quasi-simultaneous scheme. The methodology is applied to the LANN and the AGARD wing test cases. Overall, the present approach is found to improve the prediction of the aerodynamic pressure loads and of the transonic flutter dip. The main next step consists in integrating the methodology into an optimization framework in order to calculate flutter constraint quickly.

Keywords: Aeroelasticity, Aerodynamics, Aircraft design, Panel method, Viscous-inviscid interaction

1. Introduction

In order to reduce aircraft fuel burn and to improve the reliability of the design process, aerostructural optimization is nowadays carried out during the preliminary design stage. Because there is a high degree of freedom during the early design stages and since the aerodynamic modeling is the main contributor to computational cost, selecting the appropriate numerical method is of paramount importance in order to obtain results quickly with adequate accuracy. Within this context, unsteady aerodynamics is usually modeled using the Doublet Lattice Method (DLM) [1, 2], which neglects the camber, thickness and dihedral of the wing, as well as nonlinear viscous and transonic effects. As a result, traditional software such as NASTRAN [3] and ZAERO [4], must correct DLM analyses for transonic flow effects, and sometimes geometry. Alternatively, the Source and Doublet Panel Method (SDPM) [5, 6, 7, 8, 9] can predict aerodynamic loads on the actual wing geometry. As a consequence, the SDPM needs to be corrected only for nonlinear flow effects. More specifically, the unsteady pressure loads obtained using the panel method can be corrected using higher-fidelity steady pressure distributions, embedding viscous and transonic physics [10, 11]. These steady results are typically obtained by solving the Reynolds-Averaged Navier-Stokes equations [12, 13]. However, such calculations can be complex to set up and too computationally expensive for preliminary design. The viscous-inviscid interaction method [14, 15, 16, 17], whereby an inviscid flow solution is solved simultaneously with the integral boundary layer equations, can be used instead at a lower computational cost. The goal of this work is to implement and demonstrate such a correction for calculating unsteady aerodynamic loads and predicting flutter in the transonic flow regime. First, the SDPM will be used to calculate the unsteady surface pressure loads acting on the LANN wing undergoing a forced pitching motion. In order to capture transonic effects, the SDPM will be corrected by a recently developed transonic correction technique [10], whereby the steady pressures have been obtained by a novel viscous-inviscid interaction method [17]. Then, the SDPM will be coupled to a structural solver

and a $p-k$ method in order to compute the flutter speed of the AGARD wing at several freestream Mach numbers. In both cases, the results will be compared against experimental data. Section 2 presents the overall methodology and briefly describes the aeroelastic, structural and aerodynamic models and methods used in this work. Section 3 demonstrates the results obtained for the aerodynamic and aeroelastic test cases. Finally, section 4 concludes the present work by highlighting the main points and suggesting directions for future work.

2. Methodology

Figure 1 shows an overview of the computational framework used to carry out aeroelastic analysis. The different components are then briefly described in the following section.

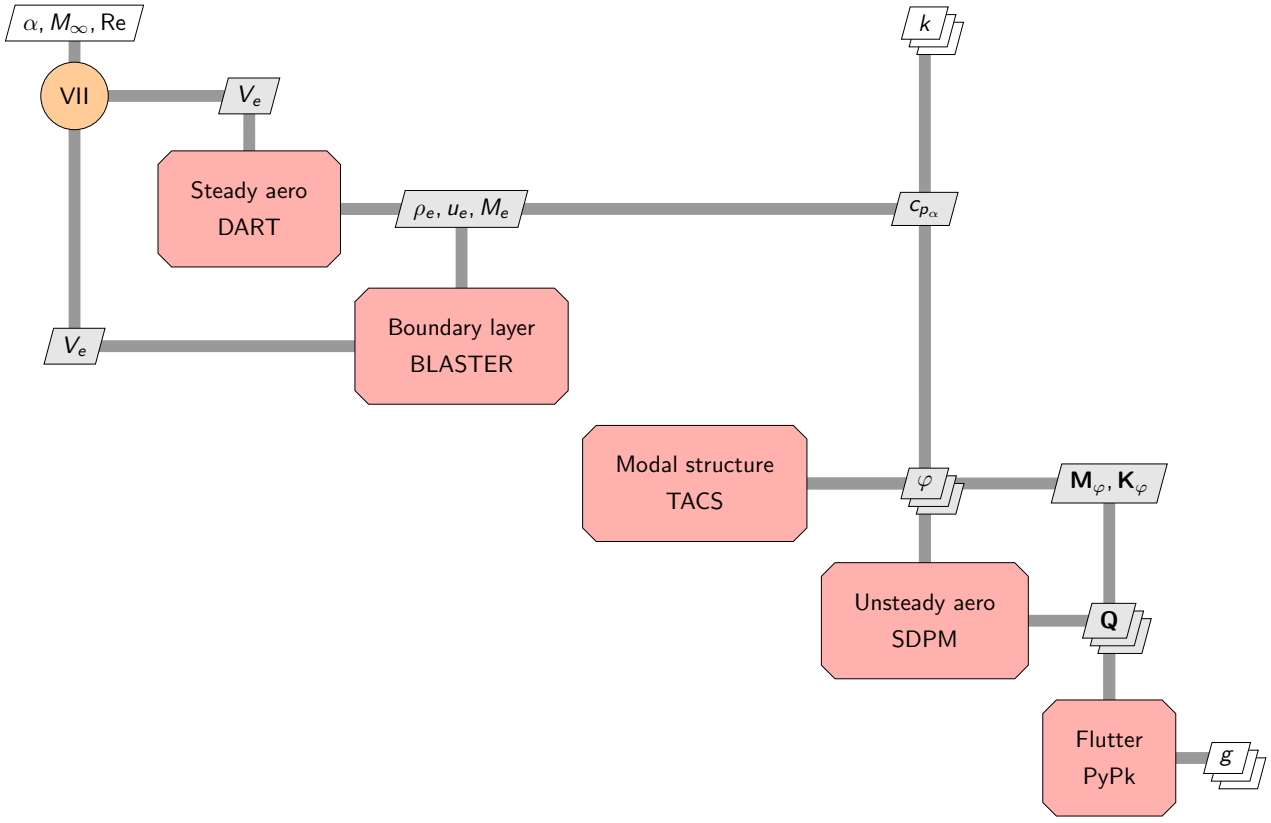

Figure 1 – Overview of the aeroelastic analysis framework.

The process starts by calculating two steady aerodynamic solutions around a given angle of attack α, at a freestream Mach number M_∞ and a Reynolds number Re. The full potential solver `DART` [18] [1] is coupled to the boundary layer solver `BLASTER` [17] [2] through the viscous-inviscid interaction methodology. `BLASTER` uses the density ρ_e, tangent velocity u_e and Mach number M_e computed by `DART` on the wing surface, and calculates a blowing velocity V_e which is then fed back to `DART` as a boundary condition. Once the viscous-inviscid interaction process has converged, the derivative of the surface pressure coefficient with respect to the angle of attack, c_{p_α}, is computed using finite differences. Flutter is then calculated by coupling the structural solver `TACS` [19] [3], the panel method `SDPM` [10] [4] and the $p-k$ solver `PyPk` [5]. The modal analysis method implemented in `TACS` [20] is first used to calculate the mode shapes φ of the structure and the reduced modal mass and stiffness matrices $\mathbf{M}_\varphi$ and $\mathbf{K}_\varphi$. The mode shapes are then used as a boundary condition in `SDPM` in order to calculate the gener-

[1] `https://gitlab.uliege.be/am-dept/dartflo`, accessed May 2024.
[2] `https://gitlab.uliege.be/am-dept/blaster`, accessed May 2024.
[3] `https://github.com/smdogroup/tacs`, accessed May 2024.
[4] `https://gitlab.uliege.be/am-dept/sdpm`, accessed May 2024.
[5] `https://gitlab.uliege.be/am-dept/pypk`, accessed May 2024.

alized aerodynamic force matrices $\mathbf{Q}$ at several reference reduced frequencies k. These matrices are corrected using the steady pressure derivatives c_{p_α} in order to model transonic flow nonlinearities. Finally the structural and aerodynamic matrices are given to `PyPk`, which implements a collection of $p-k$ methods [21, 22], and is used to calculate the aeroelastic damping g. Note that, because the computations are performed by various software using a segregated approach, the data must be transferred from one solver to another using interpolation. More specifically, radial basis functions are used to interpolate the data between `DART` and `BLASTER`, and between `TACS` and `SDPM`.

2.1 Structural modeling

Including the full dynamics of the structure directly in a flutter solution method can be prohibitively expensive for realistic structures. In order to decrease the computational cost, the structural problem is expressed in the frequency domain. Assuming harmonic motion, the equation governing the structural dynamics is cast into the modal equation

$$(\mathbf{K} - \omega_i^2 \mathbf{M})\varphi_i = 0, \tag{1}$$

where $\mathbf{M}$ and $\mathbf{K}$ are the structural mass and stiffness matrices originating from a finite element discretization of the structure, and where ω_i and φ_i are the natural frequencies and the mode shapes of the structure. The shift and invert Lanczos frequency analysis method implemented in `TACS` [20], a finite element code developed at Georgia Tech, is used to solve equation 1. The reduced modal mass and stiffness matrices $\mathbf{M}_\varphi$ and $\mathbf{K}_\varphi$ are calculated by retaining the first few mode shapes of the structure as

$$\begin{aligned} \mathbf{M}_\varphi &= \Phi^T \mathbf{M} \Phi = \mathbf{I}, \\ \mathbf{K}_\varphi &= \Phi^T \mathbf{K} \Phi = \mathrm{diag}(\omega_i^2), \end{aligned} \tag{2}$$

where Φ is a matrix containing the corresponding mode shapes.

2.2 Unsteady aerodynamic modeling

The unsteady compressible Source and Doublet Panel Method implemented in `SDPM` [10] solves the linearized potential flow equation scaled for subsonic compressible flow. In order to reduce the computational cost, the equation is expressed in the frequency domain. After discretizing the surface of the wing into quadrilateral panels, each holding a constant-strength source and doublet distribution, Green's theorem becomes

$$\mathbf{A}(k)\mu(k) = \mathbf{B}(k)\sigma(k), \tag{3}$$

where k is the reduced frequency, σ and μ are the source and doublet strengths, and $\mathbf{A}$ and $\mathbf{B}$ are the compressible influence coefficient matrices. The wing surface is modeled as quasi-fixed, *i.e.* the wing geometry is constant and the motion of the wing due to rigid or flexible oscillations is taken into account by imposing the relative attitude and motion between the surface and the fluid as a boundary condition. The source strength on each panel is evaluated by enforcing zero mass flux normal to the surface. The doublet strength is then obtained by solving Equation 3. The sources and doublets are then differentiated on the surface to compute the velocity which is in turn used to calculate the surface pressure coefficient. The pressure coefficient is then integrated on the surface to obtain the pressure loads. Finally, the generalized aerodynamic force matrix at reduced frequency k is calculated by multiplying the z-component of the surface displacement δ_{z_i} of mode i by the z-component of the pressure loads of mode j,

$$Q_{ij}(k) = \delta_{z_i}(k) \cdot \mathbf{c_p}_j(k) \odot \mathbf{n}_z \odot \mathbf{S_p}, \tag{4}$$

where $\mathbf{c_p}_j$, $\mathbf{n}_z$, $\mathbf{S_p}$ are the vectors containing the unsteady pressure coefficients due to mode j, the z-component of the unit vectors normal to the wing and the panel surfaces, respectively, and where $\odot$ denotes the Hadamard product.

Since the panel method is based on a linear equation, it cannot model the boundary layer and shocks, which are highly nonlinear. The SDPM is corrected to account for these effects by applying correction factors to the pressure coefficient calculation [10]. The following equation must be solved to obtain the correction factors

$$\nabla \mathbf{N}_x \mathbf{D}^{\mathrm{corr}} \mathbf{A}^{-1}(0)\mathbf{B}(0)\mathbf{n}_z = \frac{\sqrt{1-M_\infty^2}}{2}\mathbf{c_p}_\alpha - \mathbf{n}_x \odot \mathbf{n}_z \cos\beta, \tag{5}$$

where $\mathbf{D}^{\text{corr}}$ is the unknown diagonal correction matrix, β is the angle of side slip, $\nabla\mathbf{N}_x$ is a matrix containing the x-component of the surface gradient operators, $\mathbf{c}_{\mathbf{p}_\alpha}$ is the vector containing the derivatives of the steady pressure coefficient with respect to the angle of attack obtained from a reference steady solution, and where $\mathbf{n}_x$ contains the x-component of the unit vectors normal to the wing surface on each panel.

2.3 Steady aerodynamic modeling

The reference steady solutions are obtained by means of viscous-inviscid interaction. The methodology couples the inviscid full potential solver `DART` [18] to the recently developed compressible pseudo-unsteady boundary layer solver `BLASTER` [17] using a novel pseudo-unsteady quasi-simultaneous iterative procedure. This approach capitalizes on the favorable mathematical properties of time-dependent equations in high-pressure gradient areas, ensuring stability in simulating mildly separated and transonic flows. This procedure was shown to provide adequate results on wings in transonic flows at a fraction of the cost of solving the Reynolds-Averaged Navier-Stokes equations and is selected in order to reduce the overall computational cost. `DART` is first used to solve the full potential equation

$$\nabla\cdot(\rho\nabla\phi)=0, \tag{6}$$

where ϕ is the velocity potential. The fluid density ρ is given by the isentropic flow relationship,

$$\rho=\rho_\infty\left[1+\frac{\gamma-1}{2}M_\infty^2\left(1-|\nabla\phi|^2\right)\right]^{\frac{1}{\gamma-1}}, \tag{7}$$

where ρ_∞ is the freestream density, γ is the heat capacity ratio and M_∞ is the freestream Mach number. A transpiration boundary condition is enforced to solve equation 6, whereby the velocity normal to the wing surface is prescribed as the blowing velocity. The density ρ_e, the velocity u_e and the Mach number M_e on the wing surface are then transferred to `BLASTER`, which solves an unsteady integral form of the boundary layer equations [14]

$$\frac{H}{u_e}\frac{\partial\theta}{\partial t}+\frac{\theta}{u_e}\frac{\partial H}{\partial t}+\frac{\theta H}{u_e^2}\frac{\partial u_e}{\partial t}=\frac{\partial\theta}{\partial\xi}+(2+H-M_e^2)\frac{\theta}{u_e}\frac{\partial u_e}{\partial\xi}-\frac{c_f}{2}, \tag{8}$$

$$\begin{aligned}&\frac{1+H(1-H^*)}{u_e}\frac{\partial\theta}{\partial t}+\frac{\theta(1-H^*)}{u_e}\frac{\partial H}{\partial t}+\frac{\theta(2-H^*H)}{u_e^2}\frac{\partial u_e}{\partial t}\\&=\theta\frac{dH^*}{d\xi}+(2H^{**}+H^*(1-H))\frac{\theta}{u_e}\frac{\partial u_e}{\partial\xi}-2c_d+H^*\frac{c_f}{2},\end{aligned} \tag{9}$$

where ξ is the curvilinear coordinate along the airfoil surface, θ is the momentum thickness of the boundary layer, H is the shape factor, c_f and c_d are the local friction and dissipation coefficients defined at the wall, and where H^* and H^{**} are the kinetic energy and density shape parameters. Note that the boundary layer equations 8 and 9 are one-dimensional and are solved on strips located along the span of a three-dimensional wing. When the flow is laminar, the e^N method [23, 24] is used to predict transition. Equations 8 and 9 are solved together with a third equation representing the unsteady evolution of the amplification ratio N [17]

$$\frac{\partial N}{\partial t}+\frac{\partial N}{\partial\xi}=\left(\frac{\mathrm{d}N}{\mathrm{dRe}_\theta}\frac{\mathrm{dRe}_\theta}{\mathrm{d}\xi}\right)_{\text{attached}}+A_{\text{separated}}, \tag{10}$$

where $A_{\text{separated}}$ modifies the envelope amplification rate in separated flows. When the flow is turbulent, equations 8 and 9 are solved together with the shear-lag equation [14]

$$\begin{aligned}&\frac{\delta}{U_s u_e C_\tau}\frac{\partial C_\tau}{\partial t}+\frac{2\delta}{U_s u_e^2}\frac{\partial u_e}{\partial t}+\frac{\delta}{C_\tau}\frac{dC_\tau}{d\xi}\\&=5.6\left(C_{\tau_{EQ}}^{1/2}-C_\tau^{1/2}\right)+2\delta\left\{\frac{4}{3\delta^*}\left[\frac{c_f}{2}-\left(\frac{H_k-1}{6.7H_k}\right)^2\right]-\frac{1}{u_e}\frac{du_e}{d\xi}\right\},\end{aligned} \tag{11}$$

where δ is the boundary layer thickness, δ^* is the displacement thickness, C_τ is the shear-stress coefficient, $C_{\tau_{EQ}}$ is the equilibrium shear-stress coefficient, H_k is the kinematic shape parameter and U_s is the equivalent normalized wall slip velocity, computed using an empirical correlation. The blowing velocity V_e can finally be computed as

$$V_e = \frac{1}{\rho_e}\frac{d}{dx}\left(\rho_e u_e \delta^*\right), \tag{12}$$

and transferred to DART where it is used as a transpiration boundary condition on the wing surface.

2.4 Flutter solution method

Aeroelastic stability is assessed by caclulating the aeroelastic eigenvalues of the system, which can be found by solving the flutter equation

$$\left[2\frac{u_\infty^2}{c}p_i^2\mathbf{M}_\varphi + \mathbf{K}_\varphi - \frac{1}{2}\rho_\infty u_\infty^2 \mathbf{Q}(k)\right]\mathbf{q}_i = 0, \tag{13}$$

where ρ_∞ and u_∞ are the freestream density and velocity, c is a reference chord length, and p_i and $\mathbf{q}_i$ are the eigenfrequencies and eigenmodes. The eigenfrequency p is expressed as

$$p = (g + \mathrm{i})k, \tag{14}$$

where k denotes the reduced frequency and g denotes the damping, and where i is the imaginary unit. Because the eigenfrequency and the generalized aerodynamic force matrix both depend on the reduced frequency, the flutter problem is implicit and must be solved iteratively. A common approach to obtain a solution to the flutter equation is to resort to the $p-k$ method [21]. In the present work, a non-iterative version of the $p-k$ method implemented in PyPk [22] is used instead. The aerodynamic matrices are first computed for a given set of reference reduced frequencies. The flutter equation is then solved once for each reduced frequency using the corresponding aerodynamic matrix. The difference between the imaginary part of the eigenfrequency solutions and the reference reduced frequencies $\delta_i = \Im(p_i) - k_i$ is then computed. Because the imaginary part of the eigenfrequency is the reduced frequency, a change in the sign of the differences δ_1 and δ_2 between two consecutive eigenfrequencies p_1 and p_2 indicates that a valid solution exists between these two eigenfrequencies. This solution can then be found by linear interpolation. Once the the imaginary part of the solution has been interpolated, the real part of the eigenfrequency can also be interpolated and the damping can be computed as well.

3. Results

3.1 Aerodynamic case: LANN wing

The methodology is applied to calculate the unsteady aerodynamic loads on the LANN wing. The half-wing has an aspect ratio of 7.9, a taper ratio of 0.4, a leading edge sweep angle of $27.5°$, a twist of $-4.8°$, a root chord of 0.36 m, a half-span of 1 m, and features a transonic airfoil. The exhaustive definition of the wing is presented in Zwaan [25]. The wing is forced to pitch harmonically around an axis located at 62.1% of the root chord at a freestream Mach number $M_\infty = 0.77$ and a Reynolds number $\mathrm{Re} = 5.22 \times 10^6$. The angle of attack follows a sinusoidal variation with semi-amplitude $\tilde{\alpha} = 0.125°$ at a frequency $2\pi \times 24$ rad/s around a mean pitch value $\alpha = 2.6°$. The reduced frequency based on the half-chord is $k = 0.11$. The meshes used to simulate the LANN wing in SDPM, DART and BLASTER are generated using Gmsh [26] [6]. For SDPM, the half-wing model is discretized using 40 quadrilateral panels along the chord and 24 along the span, on both the suction and pressure sides. For DART and BLASTER, the half-wing model is placed in a box extending 50 chord lengths away from the body. The inviscid unstructured grid is generated using a cell size of 1% of the local chord and a growth ratio of 1.1, and contains $1\,327\,000$ tetrahedral cells. The viscous grid contains 15 spanwise sections, each discretized with 85 points along the chord on the suction and pressure sides.

[6] https://gmsh.info, accessed May 2024.

Figure 2 shows the steady pressure coefficient along the chord of several spanwise sections of the LANN wing obtained using SDPM, DART/BLASTER (*abbr.* BLASTER), a Reynolds-Averaged Navier-Stokes (RANS) solution previously obtained by the authors [10] and experimental data [25]. As expected, SDPM is not able to capture the shock and predicts a smooth pressure distribution. On the other hand, the pressure distributions predicted using BLASTER are in good agreement with those obtained by the RANS calculation and those measured experimentally. Nevertheless, the pressure increase due to the shock predicted by BLASTER lies slightly downstream of, and is more gradual than, the corresponding experimental observations. The results were obtained in under 35 minutes on 4 cores of a desktop workstation equipped with an AMD 3700X processor. The BLASTER calculation is therefore significantly faster than RANS, which required more than 8 hours on 8 cores.

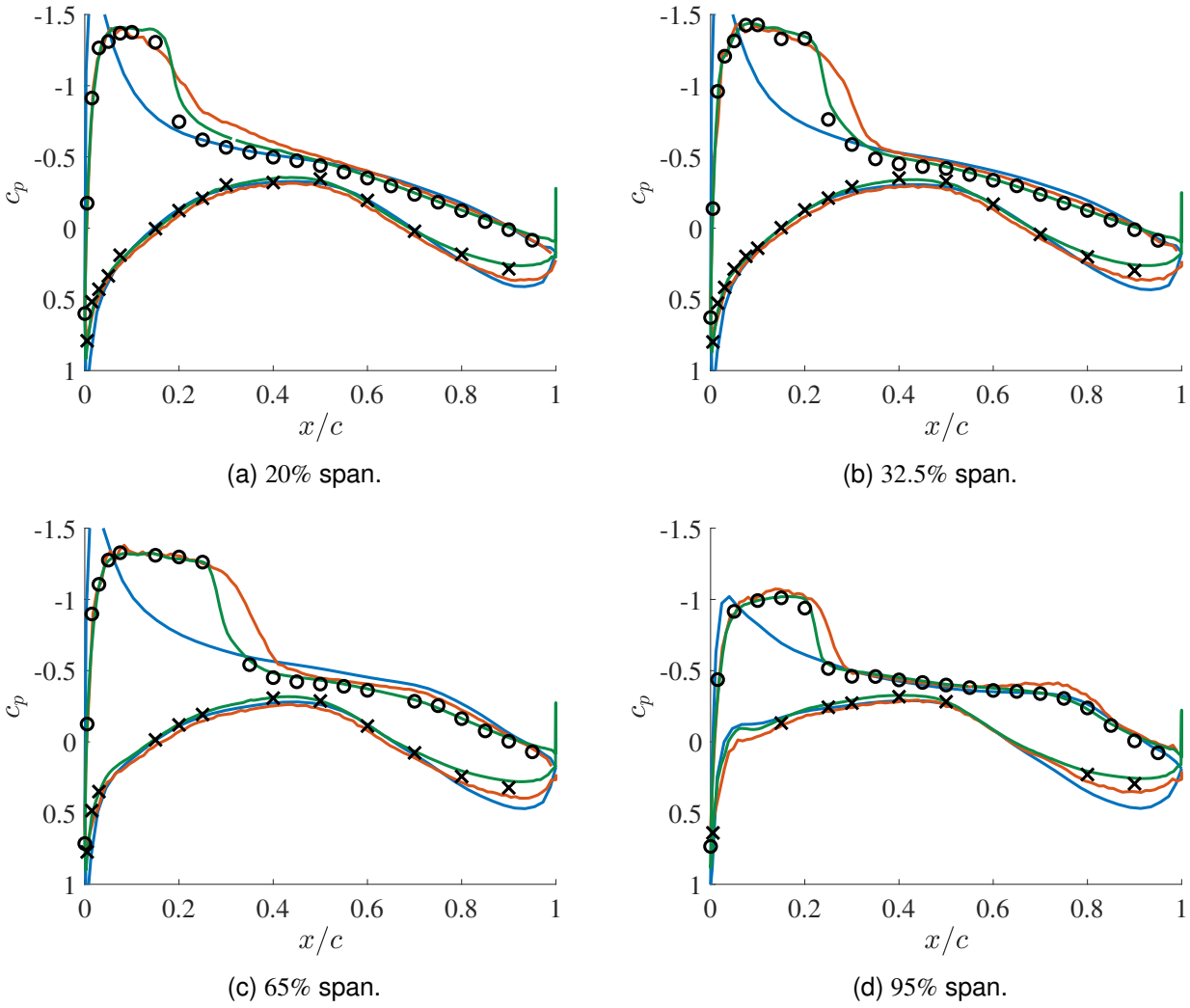

(a) 20% span.

(b) 32.5% span.

(c) 65% span.

(d) 95% span.

Figure 2 – Steady pressure coefficient along the chord of several spanwise sections of the LANN wing obtained using SDPM (blue line) and BLASTER (red line), compared to a RANS solution [10] (green line) and to the experimental data [25] (black circles and crosses for the suction and pressure sides, respectively).

Figure 3 compares the derivative of the steady pressure coefficient with respect to the angle of attack computed using BLASTER to that computed using RANS and to that obtained experimentally. The derivative is computed using finite differences between the results obtained using BLASTER at 2.59° and 2.61° angle of attack. Overall, the derivative computed using BLASTER is in good agreement with both the RANS solution and the experimental measurements, except near the shock location. The differences in the location of the peak result from the the fact that the shock predicted by BLASTER does not correspond exactly to that calculated using RANS and to that measured experimentally, as depicted in figure 2. On the other hand, the peak amplitudes computed by BLASTER seem to

lie closer to the experimental data than those obtained from RANS. Nevertheless, the derivative calculated using BLASTER is oscillatory around 65% span. Since the solution computed by BLASTER is not oscillatory, these oscillations may come from the finite difference technique used to compute the derivative. Resorting to a direct method [27] to calculate the gradient could alleviate this issue.

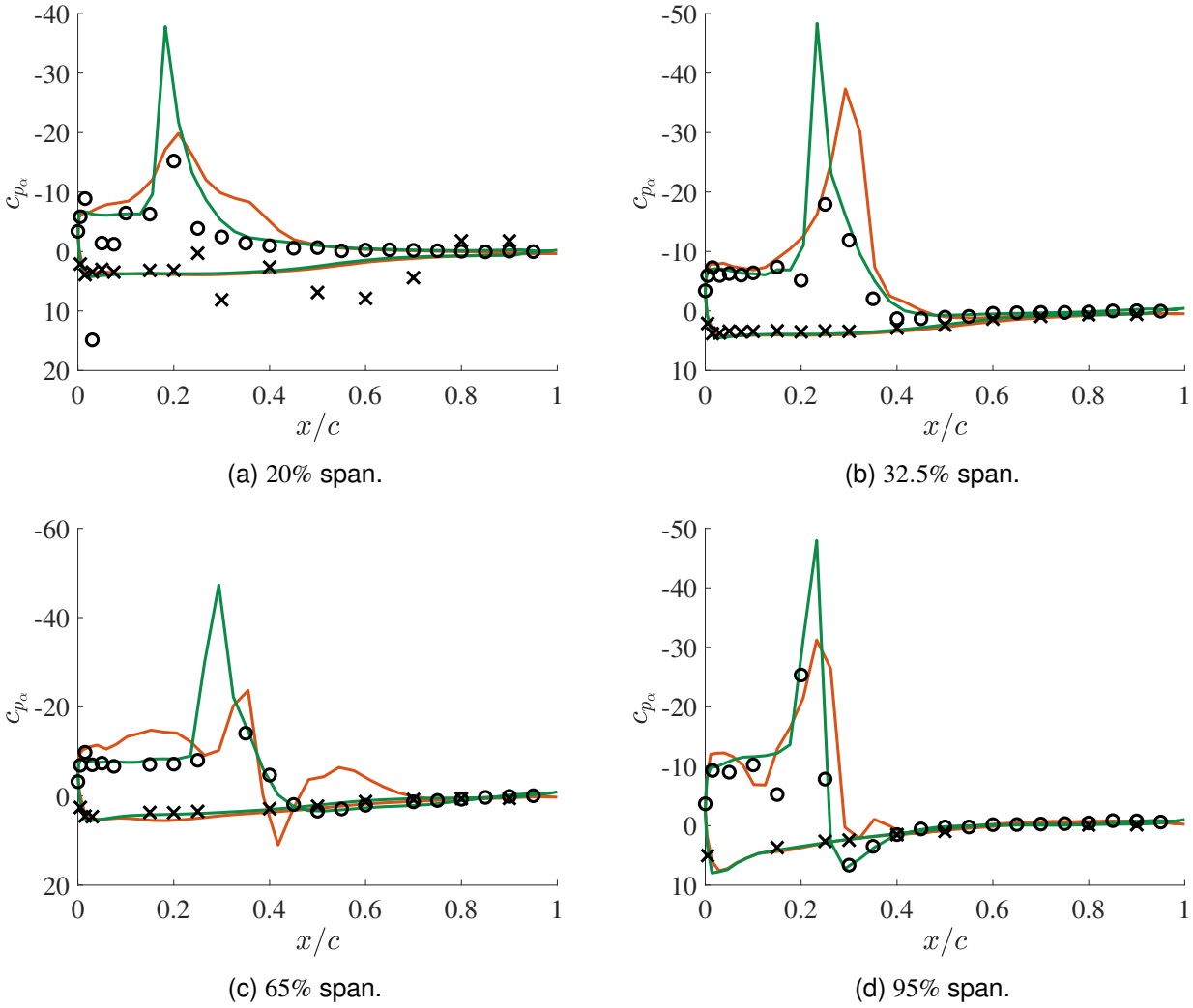

(a) 20% span.

(b) 32.5% span.

(c) 65% span.

(d) 95% span.

Figure 3 – Derivative of the steady pressure coefficient with respect to the angle of attack along the chord of several spanwise sections of the LANN wing obtained using BLASTER (red line) and compared to the RANS solution [10] (green line) and to the experimental measurements [25] (black circles and crosses for the suction and pressure sides, respectively).

Figure 4 shows the unsteady pressure distribution obtained from the uncorrected SDPM and from SDPM corrected using BLASTER. Figure 4 also compares these results to the solution previously obtained by the authors by correcting SDPM using the RANS solution and to the experimental measurements. Overall, the correction calculated using BLASTER improves the linear results predicted by SDPM. More specifically, the corrected pressure coefficients display the effect of a shock, even though its position and strength do not perfectly match the experimental data. The discrepancies in the pressure distribution between the computational results and the experimental measurements are directly related to the discrepancies in the derivative of the pressure, noted in figure 3.

3.2 Aeroelastic case: AGARD wing

The methodology is used to compute the flutter boundary of the AGARD 445.6 wing. The half-wing has a taper ratio of 0.66, a quarter-chord sweep angle of 45°, a root chord of 0.59 m, a half-span of 0.76 m, and features a symmetric NACA 65A004 airfoil. Experimental tests were conducted at several Mach numbers on a flexible weakened wing model made of mahogany and installed in a wind tunnel

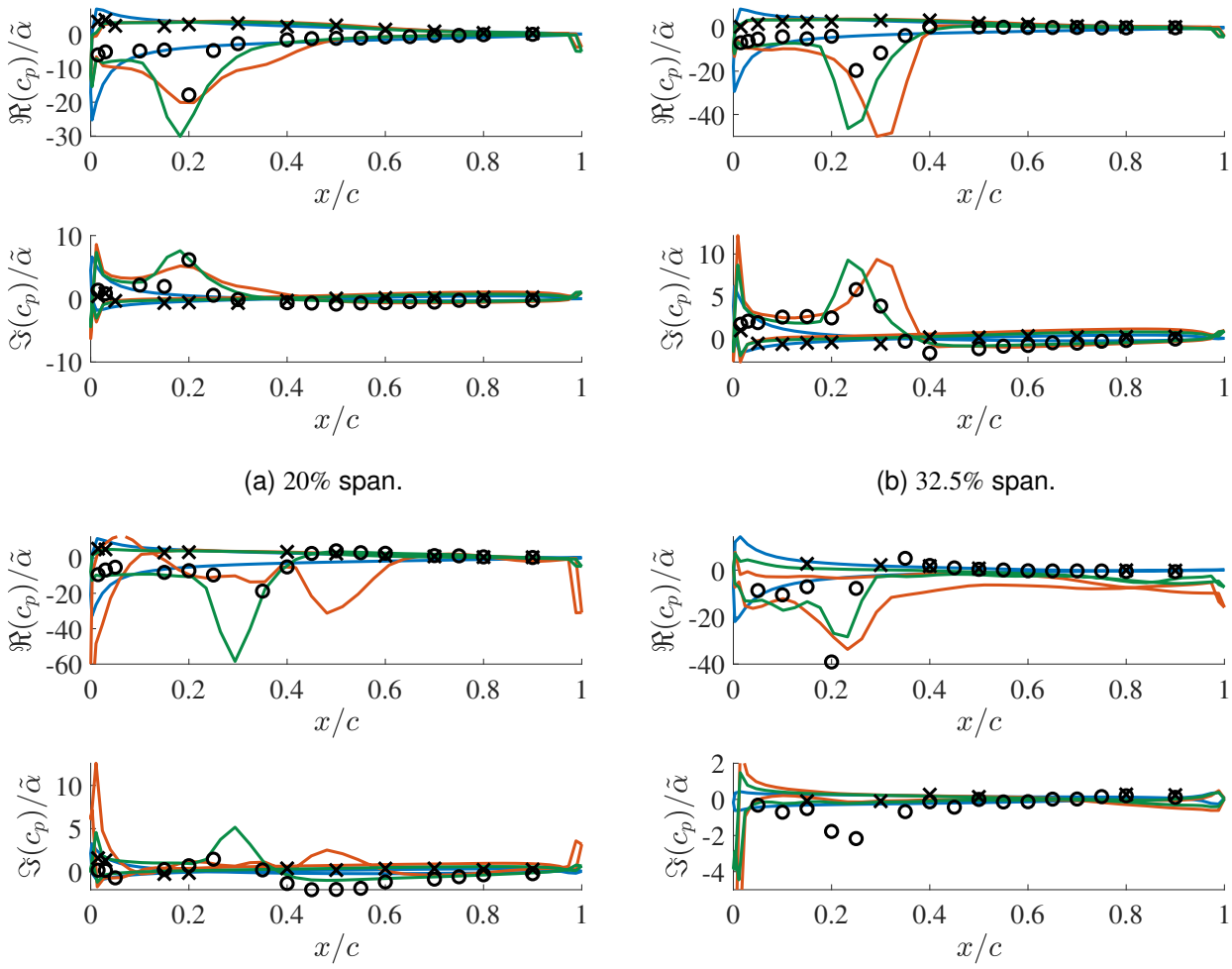

(a) 20% span.

(b) 32.5% span.

(c) 65% span.

(d) 95% span.

Figure 4 – Real and imaginary parts of the unsteady harmonic pressure coefficient along the chord of several spanwise sections of the LANN wing obtained using `SDPM`, alone (blue line) and corrected using `BLASTER` (red line), compared to the solution obtained by correcting `SDPM` using the RANS data [10] (green line) and to the experimental data [25] (black circles and crosses for the suction and pressure sides, respectively).

at an angle of attack of $\alpha = 0°$. The exhaustive definition of the test case is presented in Yates [28]. The wing is modeled as a flat plate made of shell elements in `TACS`. The longitudinal and transverse Young's modulus, the Poisson's ratio and the shear modulus are set to 3.3 GPa and 416.2 MPa, 0.31 and 439.2 MPa, respectively. The thickness of each element is defined so that it corresponds to the actual thickness of the NACA 65A004 airfoil. The grid is made of 40 quadrilateral elements along the chord and 20 along the span. The first four mode shapes and frequencies computed using `TACS` are in good agreement with those published by Yates [28]. The generalized aerodynamic force matrices are computed at four freestream Mach numbers $M_\infty = [0.5, 0.68, 0.9, 0.96]$ and at seven reference reduced frequencies $k = [0.01, 0.1, 0.2, 0.3, 0.5, 0.7, 1.0]$ using `SDPM`. The mesh is generated using `Gmsh` and counts 40 quadrilateral panels along the chord and 20 along the span, on both the suction and pressure sides of the half-wing model. The flow around the wing is subsonic except at $M_\infty = 0.90$ and $M_\infty = 0.96$, where it becomes transonic. `BLASTER` is then used to correct `SDPM` at these two Mach numbers. The Reynolds numbers corresponding to these freestream conditions are $\mathrm{Re} = 8.16 \times 10^5$ and $\mathrm{Re} = 5.96 \times 10^5$, respectively. The half-wing model is placed in a box extending 50 chord lengths away from the body. The inviscid unstructured grid is generated using a cell size of 1% of the local chord and a growth ratio of 1.1, and counts $624\,000$ tetrahedral cells. The viscous grid contains 15 spanwise sections, each discretized with 85 points along the chord on the suction and

pressure sides. BLASTER required under 3 minutes on 4 cores to run the calculation.
Figure 5 shows the flutter boundary of the AGARD wing. The flutter index u^*_{flutter} is obtained by normalizing the airspeed at flutter by the reference chord length c, the first torsion frequency ω_2 and the mass ratio between the air and the wing, μ_w,

$$u^*_{\text{flutter}} = \frac{2u_{\text{flutter}}}{c\omega_2\sqrt{\mu_w}}. \tag{15}$$

SDPM underpredicts the flutter index when there is no shock in the flow, even when the flow is transonic at $M_\infty = 0.90$. However, when there is a shock, SDPM overpredicts the flutter index and fails to capture the transonic flutter dip properly. When SDPM is corrected using the viscous-inviscid interaction implemented in BLASTER, the abrupt decrease of the flutter index is captured more adequately, although the magnitude of the difference between the corrected result and the experimental measurement is similar to that between the uncorrected result and the experimental one. This is also the case when a RANS solution is used to correct the panel method.

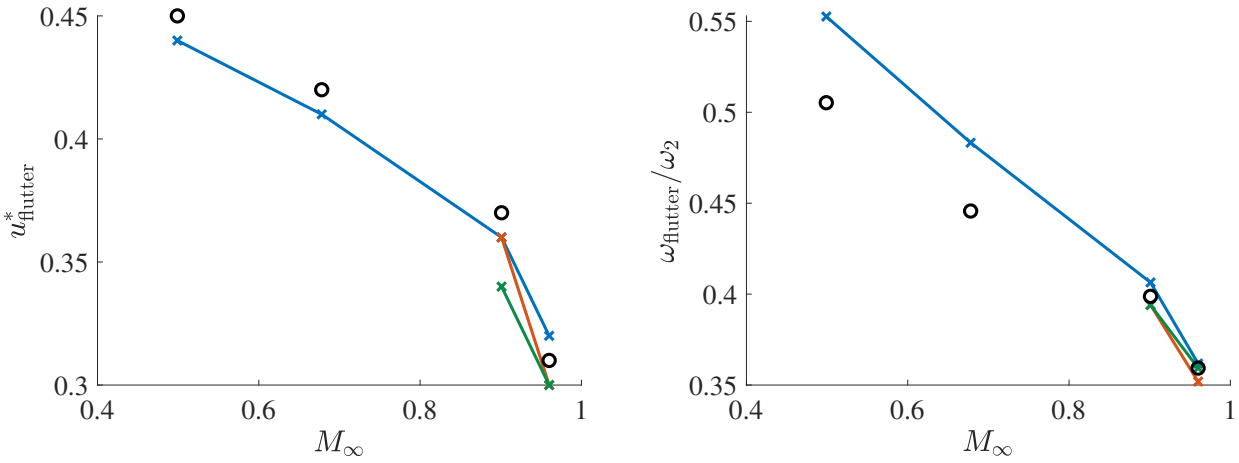

(a) Airspeed index.

(b) Frequency ratio.

Figure 5 – Flutter airspeed index and frequency ratio of the AGARD wing at several freestream Mach numbers obtained using SDPM, alone (blue line) and corrected using BLASTER (red line), compared to the solution obtained by correcting SDPM using the RANS data [10] (green line) and to experimental data [28] (black circles).

Figure 6 shows the evolution of the frequency and damping of the first four modes of the AGARD wing at a freestream Mach number $M_\infty = 0.96$ obtained using the corrected and uncorrected SDPM results. Overall, the correction brought using BLASTER has very little influence on the frequencies. However, it clearly changes the damping of the first two modes: the damping of the first bending mode increases while the damping of the first torsion mode decreases, causing flutter to appear at lower airspeed.

4. Conclusion

This work presented a new methodology for calculating unsteady aerodynamic loads and predicting flutter in the transonic regime. The approach consists in combining a transonic correction technique recently developed for the Source and Doublet Panel Method with a novel viscous-inviscid interaction technique, which couples the steady inviscid full potential equation to the unsteady integral boundary layer equations through a quasi-simultaneous scheme. The methodology was applied to two test cases and the results were compared to higher-fidelity data obtained using the RANS equations as a correction and to experimental data. The first test case was the LANN wing undergoing forced pitching oscillations. Overall, the pressure coefficients obtained using the present approach were in reasonable agreement with experimental data and showed an improvement over using the uncorrected method while maintaining a low computational cost. The second application was the AGARD

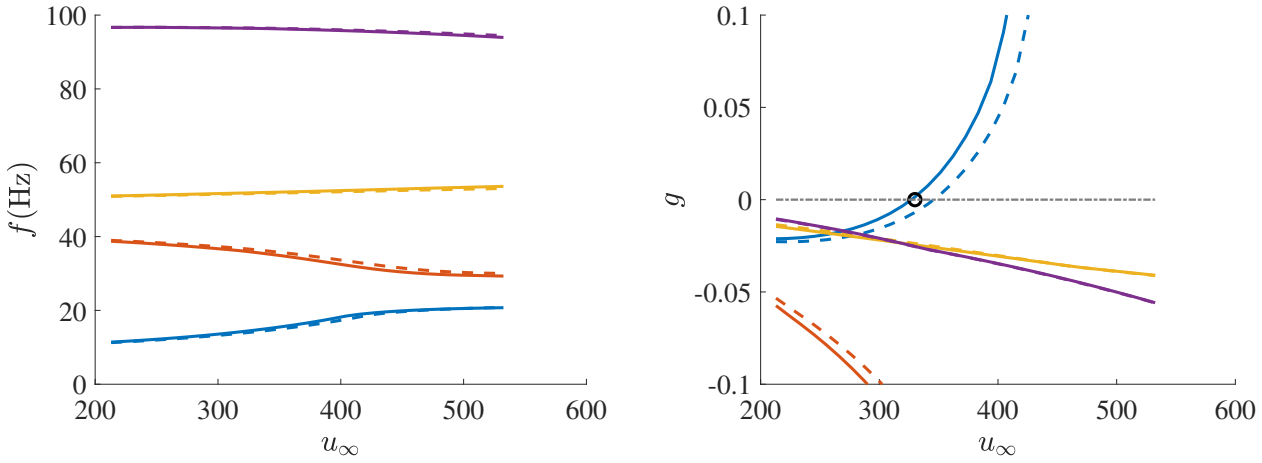

(a) Frequency.

(b) Damping.

Figure 6 – Frequency and damping of the AGARD wing as a function of the airspeed at freestream Mach number $M_\infty = 0.96$ obtained using `SDPM`, alone (dashed lines) and corrected using `BLASTER` (solid lines). The blue, red, yellow and violet lines represent the results obtained for the first bending, first torsion, second bending and second torsion modes, respectively. The dash-dotted gray line represent zero-damping and the black circle denotes the flutter speed measured experimentally.

445.6 wing test case. Using the present approach improved the prediction of the transonic flutter dip phenomenon. Even though the present methodology was found to improve the predictions of the source and doublet panel method in the transonic regime, some discrepancies with the experimental and higher-fidelity data were observed. These discrepancies have two sources. Firstly, the shock predicted by the viscous-inviscid interaction technique may not lie at the same place as that predicted by higher-fidelity models or that measured experimentally. Consequently, the derivative of the pressure coefficient with respect to the angle of attack will be affected, as well as the corrected unsteady results. Secondly, because the steady pressure derivative is calculated using finite differences, which are prone to numerical errors, the corrected results may be oscillatory. Resorting to a direct method to calculate the gradient may alleviate the issue. Finally, this work showed that the present methodology can be used to calculate flutter in the transonic regime at a low computational cost. Consequently, additional future work consists in integrating the present approach into an optimization framework to enforce flutter constraints.

5. Contact Author Email Address

a.crovato@uliege.be

6. Copyright Statement

References

[1] Albano E. and Rodden W.P. A Doublet-Lattice Method for calculating lift distributions on oscillating surfaces in subsonic flows. *AIAA Journal*, 7(2):279–285, 1969.

[2] Kalman T.P., Rodden W.P., and Giessing J.P. Applications of the Doublet-Lattice Method to nonplanar configurations in subsonic flows. *AIAA Journal*, 8(6):406–413, 1971.

[3] Rodden W. and Johnson E. *MSC/NASTRAN Aeroelastic Analysis User Guide*. MSC Software, 1994.

[4] Zona Technology. *ZAERO User Manual*, 2017.

[5] Morino L. A general theory of unsteady compressible potential aerodynamics. Technical report, NASA, 1974.

[6] Morino L. and Chen P.C. Steady and oscillatory subsonic and supersonic aerodynamics around complex configurations. *AIAA Journal*, 13:368–374, 1975.

[7] Sánchez Martínez Mariano and Dimitriadis Grigorios. Subsonic source and doublet panel methods. *Journal of Fluids and Structures*, 113:103624, 2022.

[8] Dimitriadis G. *Unsteady aerodynamics - potential and vortex methods*. Wiley, 2023.

[9] Dimitriadis G., Panagiotou P., Dimopoulos T., and Yakinthos K. Aerodynamic stability derivative calculations using the compressible source and doublet panel method. *under review by Journal of Aircraft*, 2024.

[10] Dimitriadis G., Crovato A., Sánchez Martínez M., Laraspata V., Soria L., Kilimtzidis S., and Kostopoulos V. Transonic corrections for the unsteady compressible Source and Doublet Panel Method. *submitted to Journal of Aircraft*, 2024.

[11] Crovato A., Kilimtzidis S., Sánchez Martínez M., and Dimitriadis G. Transonic corrections for the unsteady compressible Source and Doublet Panel Method. In *Proceedings of the Science and Technology Forum and Exposition*, Orlando, Florida, January 2024. AIAA SciTech.

[12] Wright J.R. and Cooper J.E. *Static Aeroelasticity and Flutter*, chapter 22, pages 475–480. John Wiley and Sons, 2015.

[13] Palacios R., Climent H., Karlsson A., and Winzell B. Assesment of strategies for correcting linear unsteady aerodynamics using cfd or test results. In *Proceedings of the International Forum on Aeroelasticity and Structural Dynamics*, Madrid, Spain, June 2017. IFASD.

[14] Drela M. and Giles M.B. Viscous-inviscid analysis of transonic and low Reynolds number airfoils. *AIAA Journal*, 25(10):1347–1355, 1987.

[15] Dechamps P., Bilocq A., Crovato A., Dimitriadis G., and Terrapon V.E. Pseudo-unsteady, quasi-simultaneous, two-dimensional interactive boundary layer methodology for preliminary aircraft design. In *Proceedings of the 8th international conference on Avdanced COmputational Methods in ENgineering*, Liège, Belgium, September 2022. ACOMEN.

[16] Dechamps P., Crovato A., Dimitriadis G., and Terrapon V.E. Three-dimensional pseudo-unsteady viscous-inviscid interaction for finite wings in transonic flow. In *Proceedings of the Science and Technology Forum and Exposition*, Orlando, Florida, January 2024. AIAA SciTech.

[17] Dechamps Paul, Bilocq Amaury, Crovato Adrien, Dimitriadis Grigorios, and Terrapon Vincent. Pseudo unsteady quasi-simultaneuous integral boundary layer methodology for preliminary aircraft design. *In preparation for submission to Journal of Aircraft*, 2024.

[18] Crovato A., Prado A.P., Cabral P.H., Boman R., Terrapon V.E., and Dimitriadis G. An adjoint full potential solver for fast aerostructural optimization in preliminary aircraft design. *Aerospace Science and Technology*, 2023.

[19] Kennedy Graeme J. and Martins Joaquim R.R.A. A parallel finite-element framework for large-scale gradient-based design optimization of high-performance structures. *Finite Elements in Analysis and Design*, 87:56–73, 2014.

[20] Jonsson Eirikur, Kenway Gaetan K., Kennedy Graeme J., and Martins Joaquim R.R.A. Development of flutter constraints for high-fidelity aerostructural optimization. In *35th AIAA Applied Aerodynamics Conference*, Denver, Colorado, June 2017. AIAA Aviation Forum.

[21] Rodden W P. and Bellinger E.D. Aerodynamic lag functions, divergence, and the british flutter method. *Journal of Aircraft*, 19(7):596–598, 1982.

[22] Rodden W. P. and Bellinger E. D. Aeroelastic divergence and aerodynamic lag roots. *Journal of Aircraft*, 38(3):586–588, 2001.

[23] van Ingen J. A suggested semi-empirical method for the calculation of the boundary layer transistion. Technical report, Delft University of Technology, 1956.

[24] Smith A.M.O. and Gamberoni N. Transition, pressure gradient and stability theory. Technical report, Douglas Aircraft Company, 1956.

[25] Zwaan R.J. Data set 9: Lann wing pitching oscillation, in compendium of unsteady measurements. Technical report, AGARD, 1985.

[26] Geuzaine Christophe and Remacle Jean-François. Gmsh: a three-dimensional finite element mesh generator with built-in pre- and post-processing facilities. *International Journal for Numerical Methods in Engineering*, 79:1309–1331, 2009.

[27] Martins Joaquim R. R. A. and Hwang John T. Review and Unification of Methods for Computing Derivatives of Multidisciplinary Computational Models. *AIAA Journal*, 51(11):2582–2599, 2013.

[28] Yates Carson Jr. E. AGARD Standard Aeroelastic Configurations for Dynamic Response I - Wing 445.6. Technical report, AGARD, 1988.